JOURNAL OF GEOPHYSICAL RESEARCH, VOL. 98, NO. B8, PAGES 14,245–14,256, AUGUST 10, 1993

Mechanics of Wedge-Shaped Fault Blocks 1. An Elastic Solution for Compressional Wedges

AN YIN

Department of Earth and Space Sciences, University of California, Los Angeles

An elastic model is developed to investigate the initiation of normal and thrust faults in thrust wedges. The model assumes frictional sliding along the base and a linear variation of shear and normal tractions with depth along the rear of the thrust wedge. Using this model, the roles of basal friction, pore fluid pressure, and wedge configuration in controlling the mechanics of thrust wedges were evaluated. The model predicts coeval development of normal and thrust faults in the same thrust wedge and a listric shape for both thrust and normal faults. In particular, lower friction favors dominantly horizontal compression in a thrust wedge, whereas higher friction can produce dominantly horizontal extension. Wedges bounded by steep thrusts ($> 45^o$) are more likely to experience extension regardless of their sizes and the boundary conditions applied. For wedges bounded by shallow-dipping thrusts ($< 15^o$) and under the same boundary conditions, shorter wedges are more dominated by compression than longer wedges. Using this model, the length of a Hubbert-Rubey thrust toe (defined as the length of the unfractured, frontal portion of a thrust wedge) is calculated. With the same boundary conditions and mechanical properties, a thinner wedge, in general, favors a longer Hubbert-Rubey toe than a thicker wedge. This simple model is applied to explain the initiation of the short-lived Miocene normal fault system in the Higher Himalaya as a consequence of a rapid release of pore fluid pressure along the Main Central Thrust during the formation of two-mica leucogranites in the hanging wall. It also simulates the occurrence of normal faults associated with the El Asnam thrust-type earthquake.

INTRODUCTION

In the last three decades, considerable effort has been devoted to the understanding of thrust-wedge mechanics [*Price*, 1973a; *Elliott*, 1976; *Chapple*, 1978; *Davis et al.*, 1983; *Stockmal*, 1983; *Emerman and Turcott*, 1983; *Dahlen*, 1984; *Platt*, 1986; *Yin*, 1986, 1988; *Fletcher*, 1989; *Liu and Ranalli*, 1992]. These studies provide many insights into the relationships among stress distribution, boundary conditions, wedge geometry, and wedge rheology. However, two important features commonly associated with the development of thrust wedges remain little investigated. First, thrusts and normal faults commonly develop in different parts of the same thrust/orogenic wedge at the same time [e.g., *Platt*, 1986; *Dewey*, 1988]. For example, the north dipping normal fault system in the Higher Himalaya was developed in an orogenic wedge during the collision of India with Asia (Figure 1) [*Burg and Chen*, 1984; *Burchfiel and Royden*, 1985; *Burchfiel et al.*, 1992; *Harrison et al.*, 1992]. On a smaller scale, the structures developed during the 1980 El Asnam thrust-type earthquake in Algeria show coeval development of normal faults and thrusts in the same thrust wedge (Figure 2) [*Yielding et al.*, 1981; *Philip and Meghraoui*, 1983; *Ouyed et al.*, 1983; *King and Yielding*, 1984; *Avouac et al.*, 1992]. Although *Platt* [1986] inferred that high topographic slopes would favor extension in a thrust wedge, which in turn would lead to reduction of the slope to regain the stress state of horizontal compression, he provided neither analytical solutions nor numerical calculations. Thus it is uncertain whether Platt's suggestion applies to the whole thrust wedge. Second, a listric geometry has been observed in many thrust belts (Figure 3) [*Bally et al.*, 1966; it Price, 1981]. However, this is not predicted by the popular noncohesive critical Coulomb wedge model [*Dahlen*, 1984].

In order to understand the mechanics of listric thrusts and the coeval development of thrust and normal faults in the same orogenic wedge, the stress distribution in an elastic wedge was investigated. The basis for the assumed elastic constitutive relation between stress and strain is that the elastic deformation, though small, is important for the initiation of Coulomb-type fractures [*Jaeger and Cook*, 1979]. Coulomb-type fracturing, in turn, has long been considered to be the mechanism for initiation of natural faults [e.g., *Anderson*, 1942]. Another reason to assume elasticity is to compare the difference in predicted stress distributions among elastic, noncohesive Coulomb and plastic wedges that have the same boundary conditions. In doing so, the choice of constitutive relations between stress and strain for thrust wedge models can be assessed. *Liu and Ranalli* [1992] recently investigated the mechanics of elastic wedges, but because they did not specify the basal boundary condition (i.e., the shear and normal tractions on the basal thrust) of the wedge considered, their solution is not unique.

The purpose of this paper is to investigate the mechanical conditions for the intiation of both normal and/or thrust faults in thrust wedges. It is the first of two papers investigating the mechanics of wedge-shaped, elastic fault blocks. Here we are only concerned with compressional wedges bounded by thrusts at their bases. In contrast, if wedge-shaped fault blocks are bounded by normal faults at their bases, they are extensional wedges. This definition is similar to that of *Xiao et al.* [1991] for compressional and extensional Coulomb wedges.

THEORY

Stress Distribution in Thrust Wedges

The geometry of an elastic-brittle thrust wedge and the framework of reference used in the calculations are shown in Figure 4, where α is the surface slope, β is the dip angle

Paper number 93JB00555.
0148-0227/93/93JB-00555$05.00

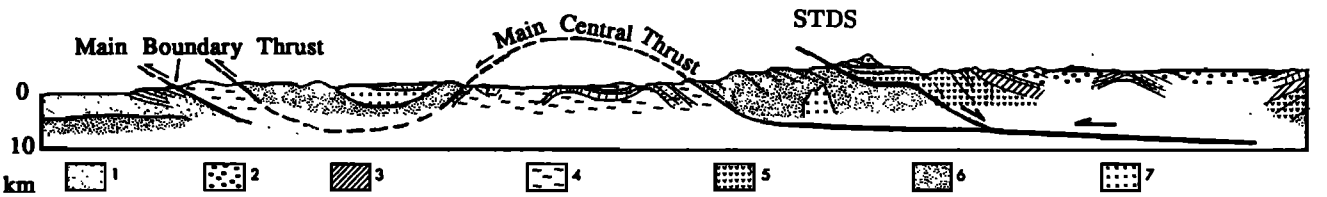

Fig. 1. Geologic cross section through the Himalaya, simplified from *Gansser* [1964] and *Lyon-Caen and Molnar* [1983]. STDS, south Tibetan detachment system of *Burchfiel et al.* [1992], is a north dipping normal fault system in the Higher (Greater) Himalaya that was coeval with the Main Central Thrust below. 1, Tertiary and Quaternary sedimentary rocks; 2, Mesozoic Indus flysch; 3, Paleozoic sedimentary rocks of Greater Himalaya; 4, Paleozoic sedimentary rocks of Lesser Himalaya; 5, upper Precambrian and lower Paleozoic sedimentary rocks; 6, Precambrian basement; 7, Himalayan leucogranites.

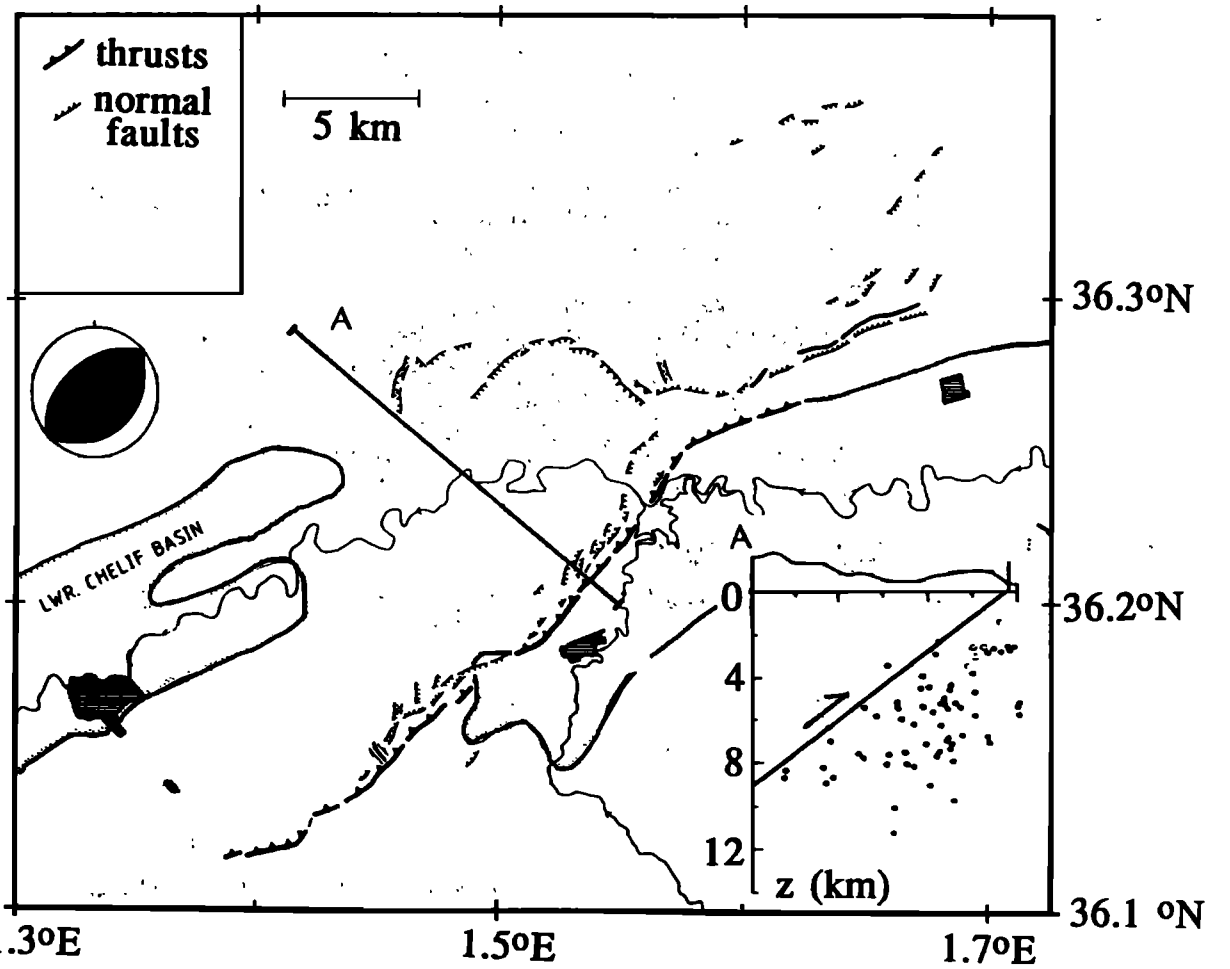

Fig. 2. Surface structures developed during the 1980 El Asnam (Algeria) thrust-type earthquake [after *King and Yielding*, 1984]. Cross section A shows the possible geometry of the main thrust as defined by the distribution of aftershocks (see *Ouyed et al.* [1983] for details).

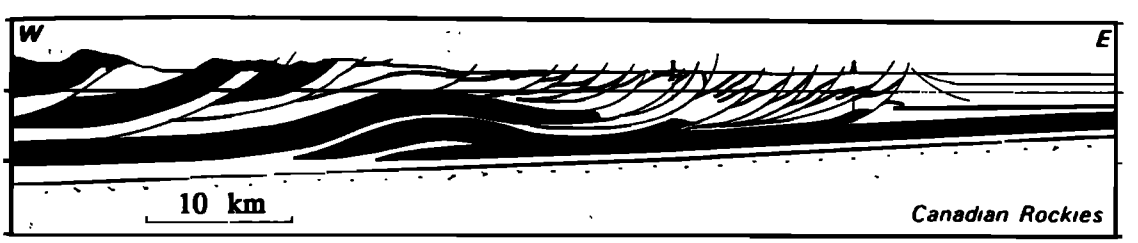

Fig. 3. Simplified geologic map of southern Canadian Rockies fold-and-thrust belt [after Bally et al., 1966]. Note that listric thrusts are common features in the cross section.

of the basal thrust, $\theta = \alpha + \beta$, and x_0 is the length of the wedge. Note that the x axis is parallel to the surface and points in the upslope direction. The sign convention follows that of elasticity, that is, tensile stress is positive.

The stress equilibrium equations of a continuum in the x and y directions for a plane stress condition are

$$\frac{\partial \sigma_{xx}}{\partial x} + \frac{\partial \sigma_{xy}}{\partial y} + X = 0 \tag{1}$$

$$\frac{\partial \sigma_{xy}}{\partial x} + \frac{\partial \sigma_{yy}}{\partial y} + Y = 0 \tag{2}$$

where σ_{xx}, σ_{yy}, and σ_{xy} are normal and shear stress components in the x and y directions and X and Y are body forces due to gravity in the x and y directions. $X = -\rho_s g \sin\alpha$, $Y = \rho_s g \cos\alpha$, ρ_s is the average density of the rock composing the thrust wedge, and g is the acceleration of gravity. As the thrust wedge may not be dry, pore fluid pressures may exist within the rocks, in which case we consider the effect of buoyancy induced by pore fluid [*Hubbert and Rubey*, 1959],

$$X_b = \lambda \rho_w g \sin\alpha \tag{3}$$

$$Y_b = -\lambda \rho_w g \cos\alpha \tag{4}$$

where ρ_w is the density of water and λ is the ratio of the pore fluid and lithostatic pressures and is known as the pore fluid pressure ratio [*Hubert and Rubey*, 1959]. The pore fluid pressure is defined as

$$P_f = -\lambda \rho_s g h \tag{5}$$

where h is the depth from the surface measured vertically downward.

We now rewrite (1) and (2) by considering the effect of pore fluid in rocks and obtain

$$\frac{\partial \overline{\sigma}_{xx}}{\partial x} + \frac{\partial \sigma_{xy}}{\partial y} + X_e = 0 \tag{6}$$

$$\frac{\partial \sigma_{xy}}{\partial x} + \frac{\partial \overline{\sigma}_{yy}}{\partial y} + Y_e = 0 \tag{7}$$

where

$$X_e = -(1-\lambda)\rho_s g \sin\alpha = -\rho_e g \sin\alpha \tag{8}$$

$$Y_e = (1-\lambda)\rho_s g \cos\alpha = \rho_e g \cos\alpha \tag{9}$$

$\rho_e = (1-\lambda)\rho_s$ is the effective density and $\overline{\sigma}_{xx}$ and $\overline{\sigma}_{yy}$ are effective stresses in the x and y directions. It can be seen from (8) and (9) that the role of the pore fluid pressure represented by λ is to reduce the magnitude of the body force. This is the buoyancy effect discussed by *Hubbert and Rubey* [1959].

A harmonic equation can be derived by using both Hooke's law and the strain compatibility condition:

$$\nabla^2(\overline{\sigma}_{xx} + \overline{\sigma}_{yy}) = 0. \tag{10}$$

For the case of constant body forces in the x and y directions, (6), (7), and (10) can be combined into the biharmonic equation

$$\nabla^4 \Phi = 0 \tag{11}$$

where Φ is the Airy stress function [e.g., *Hafner*, 1951; *Fung*, 1965] and is related to stress components by

$$\overline{\sigma}_{xx} = \frac{\partial^2 \Phi}{\partial y^2} - X_e x \tag{12}$$

$$\overline{\sigma}_{yy} = \frac{\partial^2 \Phi}{\partial x^2} - Y_e y \tag{13}$$

$$\sigma_{xy} = -\frac{\partial^2 \Phi}{\partial x \partial y}. \tag{14}$$

The boundary conditions are a stress-free upper surface and a linear variation of normal and shear tractions with depth along the rear of the wedge, i.e.,

$$\overline{\sigma}_{yy}(x, 0) = \sigma_{xy}(x, 0) = 0 \tag{15a}$$

$$\overline{\sigma}_{xx}(x_0, y) = A + By \tag{15b}$$

$$\sigma_{xy}(x_0, y) = Cy \tag{15c}$$

where A, B, and C are prescribed constants. The boundary conditions along the rear of the wedge are based on the result of in situ stress measurements [*McGarr and Gay*, 1978], which suggests that vertical and horizontal normal stresses are generally a linear function of depth. The boundary condition along the base of the wedge is assumed to follow Amonton's law [*Jaeger and Cook*, 1979]

$$\tau_b(x, y = x\tan\theta) = -\mu_b(1-\lambda_b)\overline{\sigma}_b(x, y = x\tan\theta) \tag{16a}$$

where μ_b is the coefficient of friction along the fault plane, $\overline{\sigma}_b$ is the normal stress component across the basal thrust plane, τ_b is the shear stress component along the basal thrust plane, and λ_b is the pore fluid pressure ratio along the fault plane. $\overline{\sigma}_b$ and τ_b can be related to stress components $\overline{\sigma}_{xx}$, $\overline{\sigma}_{yy}$, and σ_{xy} along the basal plane by

$$\overline{\sigma}_b = l^2 \overline{\sigma}_{xx} + m^2 \overline{\sigma}_{yy} + 2lm\sigma_{xy} \tag{16b}$$

$$\tau_b = \sigma_{xy}(l^2 - m^2) + (\overline{\sigma}_{yy} - \overline{\sigma}_{xx})lm \tag{16c}$$

where $l = -\sin\theta$ and $m = \cos\theta$.

I have obtained a solution for the above problem by assuming that the Airy stress function has the form

$$\Phi = \frac{1}{6}k_1 x^3 + \frac{1}{2}k_2 x^2 y + \frac{1}{2}k_3 x y^2 + \frac{1}{6}k_4 y^3 + \frac{1}{6}k_5 x y^3 + \frac{1}{2}k_6 x^3 y + \frac{1}{2}k_7 x^2 + \frac{1}{2}k_8 y^2 \tag{17}$$

Using (12) to (14), this gives

$$\overline{\sigma}_{xx} = k_3 x + k_4 y + k_5 x y + k_8 + \rho_e g x \sin\alpha \tag{18}$$

$$\overline{\sigma}_{yy} = k_1 x + k_2 y + k_6 x y + k_7 - \rho_e g y \cos\alpha \tag{19}$$

$$\sigma_{xy} = -k_2 x - k_3 y - \frac{1}{2}k_5 y^2 - \frac{1}{2}k_6 x^2 \tag{20}$$

where k_1 to k_8 are constants determined by the boundary conditions. Equation (15) requires that $k_1 = k_2 = k_6 = k_7 = 0$. The remaining constants k_3, k_4, k_5, and k_8 are determined by the following constraints. First, the magnitude of the stress at the toe of the thrust wedge is assumed to be known, giving

$$\overline{\sigma}_{xx}(0,0) = k_8 = \sigma_0. \tag{21}$$

This condition is equivalent to a uniform normal stress σ_0 in the x direction applied throughout the thrust wedge. As the upper limit of the magnitude of deviatoric stress in the crust falls between 20 and 100 MPa, the value of σ_0 can be as high as 200 MPa. Constant k_5 represents the gradient of $\partial\overline{\sigma}_{xx}/\partial y$ in the x direction. As it varies little in a large region shown by the result of in situ stress measurements [*McGarr and Gay*, 1978], k_5 is assumed to be zero. Finally, k_3 can be determined by (16) as a function of k_4 and k_8

$$k_3 = \frac{-k_4 a_{12} + b_1}{a_{11}} \tag{22}$$

where

$$a_{11} = x_0[\sin 2\theta - \tan\theta \sin^2\theta + \mu_b(1-\lambda_b)\sin^2\theta] \tag{23}$$

$$a_{12} = x_0 \sin^2\theta[1 + \tan\theta\mu_b(1-\lambda_b)] \tag{24}$$

$$\begin{aligned} b_1 = {} & \rho_e g x_0 \sin\theta[(\sin\alpha\cos\theta + \cos\alpha\sin\theta) \\ & +\mu_b(1-\lambda)(\sin\alpha\sin\theta - \cos\alpha\cos\alpha)] \\ & +k_8 \sin\theta[\cos\theta + \mu_b(1-\lambda)\sin\theta] \end{aligned} \tag{25}$$

and x_0 is the length of the thrust wedge.

We can now write the stress distribution in the wedge as

$$\overline{\sigma}_{xx} = k_3 x + k_4 y + k_8 + \rho_e g x \sin\alpha \tag{26}$$

$$\overline{\sigma}_{yy} = -\rho_e g y \cos\alpha \tag{27}$$

$$\sigma_{xy} = -k_3 y \tag{28}$$

Using the boundary conditions along the rear of the wedge represented by (15*b*) and (15*c*) and comparing them with (26) and (28), we obtain the following relations

$$\overline{\sigma}_{xx}(x_0, y) = A + By = k_3 x_0 + k_4 y + k_8 + \rho_e g x_0 \sin\alpha \tag{29}$$

$$\sigma_{xy}(x_0, y) = Cy = -k_3 y \tag{30}$$

where $A = k_3 x_o + \rho_e g x_o \sin\alpha + k_8$, $B = k_4$, and $C = -k_3$. By observing that k_3 is a function of k_4 in (22), B and C are related. Thus, prescribing the value of k_4 and k_8 is equivalent to knowing the boundary conditions (i.e., the value of A and B) at the rear of the wedge. Parameter $B = k_4$ represents the gradient of $\overline{\sigma}_{xx}$ in the y direction.

Equation (16*a*) only provides the constraint on the shear traction on the basal surface. As k_3, k_4, and k_8 are known, the normal traction along this surface can be derived from (16*b*)

$$\begin{aligned} \overline{\sigma}_b(x, y = x\tan\theta) = {} & l^2(k_3 x + k_4 x\tan\theta + k_8 + \rho_e g x \sin\alpha) \\ & +m^2(-\rho_e g x \tan\theta\cos\alpha) + 2lm(-k_3 x\tan\theta). \end{aligned} \tag{31}$$

Thus equations (15), (16), (29), (30), and (31) provide a complete set of boundary conditions around a thrust wedge.

Equation (26) shows the contribution of surface slope α to creating tensile stress in the x direction by the term $\rho_e g x \sin\alpha = (1-\lambda)\rho_s g x \sin\alpha$. Because the upper limit of regional surface slope of most orogenic belts is less than 3.5° [*Davis et al.*, 1983], the range of variation caused by $\sin\alpha$ term is only between 0.0 and 0.061. In contrast, the variation of the pore fluid pressure ratio λ in the wedge is between 0.0 and 1.0, much greater than that of the surface slope term. This simple analysis indicates that surface slope is a much less important factor in producing tensile stress than pore fluid pressure, although its presence may lead to generating tensile stress.

Using (26) to (28), the principal stress directions and the maximum shear stress (i.e., deviatoric stress) can be calculated by

$$\psi = \frac{1}{2}\tan^{-1}\left(\frac{2\sigma_{xy}}{\overline{\sigma}_{xx} - \overline{\sigma}_{xx}}\right) \tag{32}$$

and

$$\tau_{max} = \sqrt{\frac{1}{4}(\overline{\sigma}_{xx} - \overline{\sigma}_{xx})^2 + \sigma_{xy}^2} \tag{33}$$

respectively, where ψ is the angle between the maximum tensile stress $\overline{\sigma}_1$ and the x axis. Using (32) and (33) and applying the Coulomb fracture criterion with the assumption that an angle of internal friction ϕ is 30°, the trajectories of predicted fault patterns and distribution of the maximum shear stress can be plotted.

Lengths of Hubbert-Rubey Thrust Toes

Commonly, a significant portion of a thrust sheet is neither faulted nor folded (e.g., see cross sections of *Bally et al.* [1966]). This phenomenon was first noted by *Reade* [1908] and later became the famous mechanical paradox for far-traveled thrust blocks [*Smoluchowski*, 1909]. The significant lengths of unfractured thrust blocks and the limited strength of rocks require that the basal friction of the thrust blocks be much lower than that determined from experimental studies. The problem led to intense debate and various theories (see summary by *Suppe* [1985]). *De Bremaecker* [1987] and *Price* [1973b, 1988] questioned the validity of the mechanical paradox. They believed that the calculations of the maximum length of thrust sheet [e.g., *Hubbert and Rubey*, 1959] based on force balance between friction along the thrust and horizontal push from behind implies an assumption that frictional slip occurs simultaneously over the entire thrust surface. They further pointed out that such thrust motion is inconsistent with the dislocation model determined from earthquake seismology. Their concerns, however, may not be justified, because the dislocation model is purely a kinematic description for rupture of a fault surface during earthquake events. The model itself puts no constraints on the mechanical conditions (i.e., stress magnitudes and mechanical properties) along the fault surface [*Aki and Richards*, 1980, pp. 799-800]. It does not imply that an unruptured part of the fault was not at the verge of frictional failure. Second, the observation of limited rupture areas during earthquake faulting does not preclude the possibility that a large thrust block can move aseismically, i.e., creep at a slow rate. Because seismicity over very short time intervals (several tens of years) may cover the entire thrust fault surface, which is the case in the Himalaya [*See-*

ber et al., 1981; *Ni and Barazangi*, 1984], an active thrust surface may be everywhere at the verge of frictional failure, so that slip can occur wherever the shear traction on the thrust exceeds the frictional strength. In the following, I assume that the basal thrust is at the verge of frictional failure everywhere. Thus the result of stress distribution in elastic wedges discussed above can be used in the calculations.

The length of a Hubbert-Rubey thrust toe, L, is defined by the horizontal distance between the point (0, 0) at the wedge tip and the point $[L/\cos\alpha, \tan\theta(L/\cos\alpha)]$ at the base of the thrust wedge. At the point $[L/\cos\alpha, \tan\theta(L/\cos\alpha)]$, the state of stress satisfies the Coulomb fracture criterion (Figure 4). This statement can be expressed as [*Jaeger and Cook*, 1979]

$$\overline{\sigma}_1[L/\cos\alpha, \tan\theta(L/\cos\alpha)] = C_0 + q\overline{\sigma}_3[L/\cos\alpha, \tan\theta(L/\cos\alpha)] \quad (34)$$

where C_0 and q are constants related to the cohesive strength, S_0, and the coefficient of internal friction, μ_ϕ, by

$$C_0 = 2S_0[(\mu_\phi^2 + 1)^{1/2} + \mu_\phi] \quad (35)$$

$$q = [(\mu_\phi^2 + 1)^{1/2} + \mu_\phi]^2 \quad (36)$$

and $\overline{\sigma}_1$ and $\overline{\sigma}_3$ are the greatest and least tensile principal effective stresses. They can be calculated by

$$\overline{\sigma}_{1,3} = \frac{1}{2}(\overline{\sigma}_{xx} + \overline{\sigma}_{yy}) \pm \sqrt{\frac{1}{4}(\overline{\sigma}_{xx} - \overline{\sigma}_{yy})^2 + \sigma_{xy}^2} \quad (37)$$

where $\overline{\sigma}_{xx}$, $\overline{\sigma}_{yy}$, and σ_{xy} may be obtained by using (22) to (24). $k_8 = 0$ is assumed, because we are interested in the length of the toe as a function of both the configuration and the strength of thrust wedges. In doing so, we obtain a self-similar solution of the stress components $\overline{\sigma}_{xx}$, $\overline{\sigma}_{yy}$, and σ_{xy}; that is,, constants k_3 and k_4 in (26), (27), and (28) can be obtained without prescribing the length of the wedge. Thus, the length of the Hubbert-Rubey toe can be calculated by inserting (35), (36), and (37) into (34)

$$L = 2C_0/\{\cos\alpha[(\overline{\sigma}_{xx} + \overline{\sigma}_{yy})(1 - q) + (1 + q)\sqrt{\frac{1}{4}(\overline{\sigma}_{xx} - \overline{\sigma}_{yy})^2 + \sigma_{xy}^2}]\} \quad (38)$$

This relation indicates that the length of the Hubbert-Rubey toe is zero for a noncohesive elastic Coulomb wedge.

RESULTS

Stress Distribution

Using the model derived above, the roles of boundary conditions and wedge configuration in controlling the stress distribution in a thrust wedge can be evaluated. The coefficients of basal friction and internal friction are assumed to be 0.7 and $\tan 30^o$, respectively, for all cases calculated below. Thus pore fluid ratios within the wedge (λ) and along the base of the thrust wedge (λ_b) are considered for the basal boundary condition. Figure 5*a* shows the predicted fault pattern in the region where the magnitude of maximum shear stress (i.e., deviatoric stress) is greater than 50 MPa. I chose $x_0 = 100$ km, dip angle $\beta = 10^0$, surface slope $\alpha = 3.5^0$, $k_4 = -1.5\rho_e g$, and $k_8 = -100$ MPa. This model shows that normal faults are favored in the upper portion of the wedge, whereas thrusts are favored in the lower part of the wedge. When λ_b decreases from 0.9 to 0.4, normal faults prevail in the entire wedge (Figure 5*b*). By lowering λ from 0.4 to 0.0 and by maintaining $\lambda_b = 0.4$, we find that the fault pattern is little changed. However, if pore fluid pressure in the wedge, λ, increases from 0.4 in Figure 5*c* to 0.8 in Figure 5*d*, thrusts in the lower part of the wedge are created, whereas normal faults remain in the upper part of the wedge.

The stress distribution in an elastic wedge is also sensitive to k_4, the gradient of $\overline{\sigma}_{xx}$ in the y direction. Figure 6*a* shows the predicted fault pattern in the region where the magnitude of deviatoric stress is greater than 10 MPa for $k_4 = -0.5\rho_e g$ with all other parameters the same as

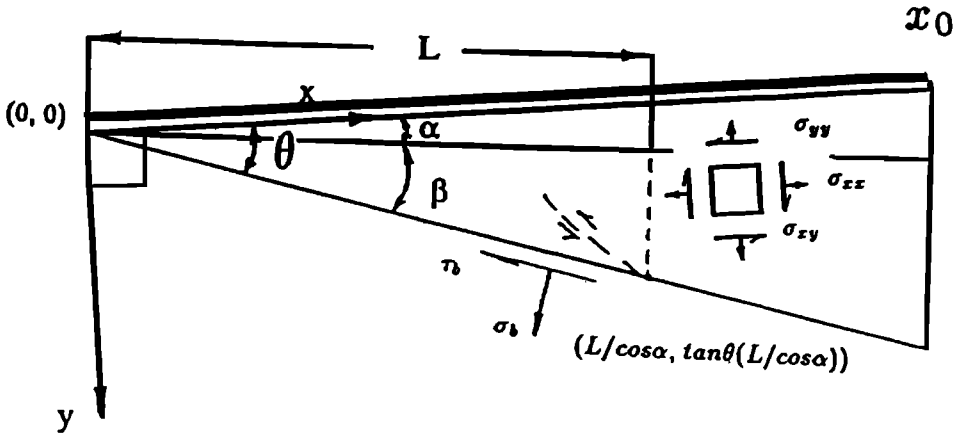

Fig. 4. Geometry of a triangular wedge, framework of reference, and sign convention used in this study. α is the surface slope, β is the dip of the basal thrust, $\theta = \alpha + \beta$, and x_0 is the length of the wedge, τ_b and σ_b are shear and normal tractions along the basal thrust, and σ_{xx}, σ_{yy}, and σ_{xy} (all have positive signs), are stress components in the x and y directions. The length of a Hubbert-Rubey toe, L, is defined by the horizontal distance between point $[L/\cos\alpha, \tan\theta(L/\cos\alpha)]$ and point (0, 0).

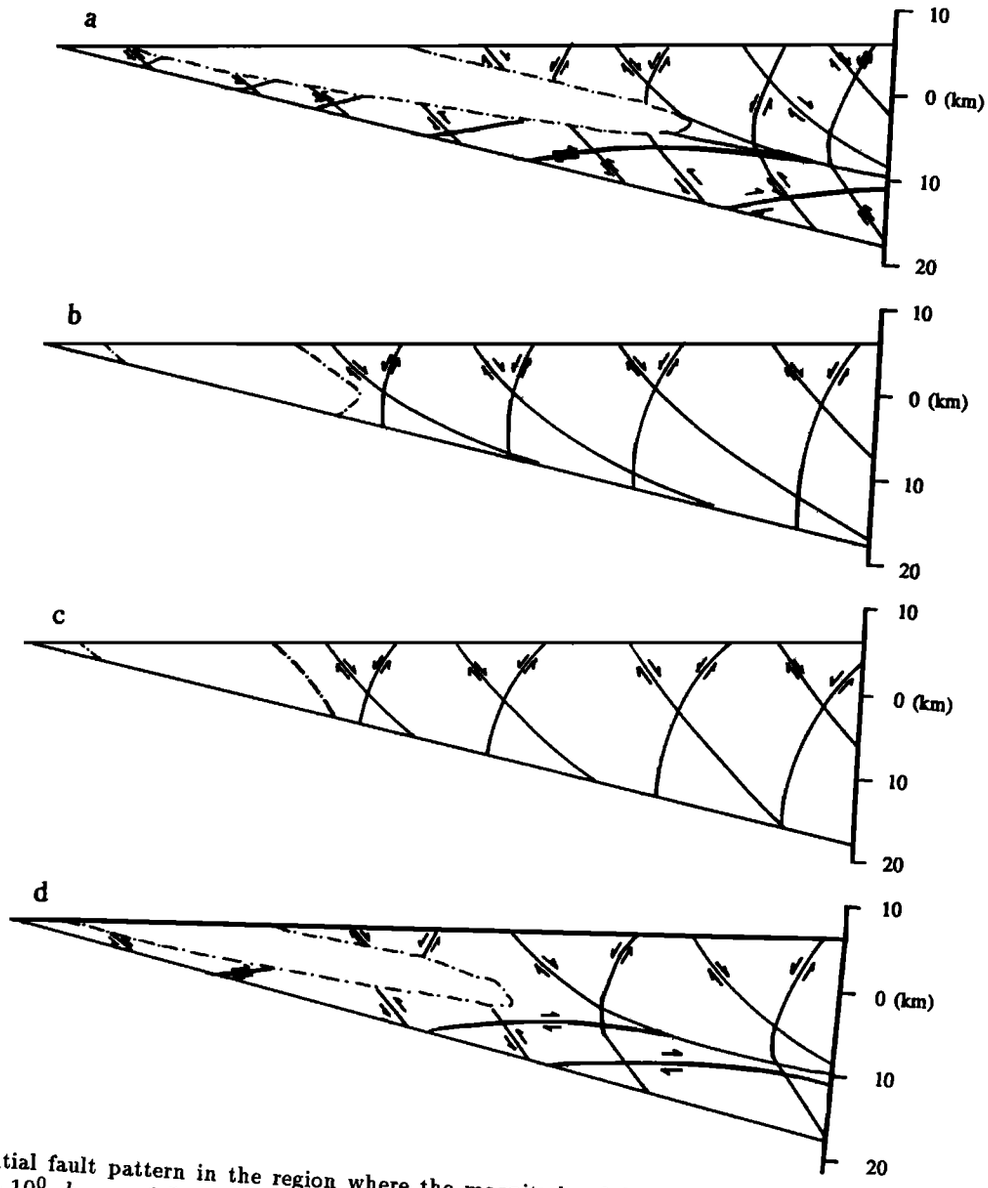

Fig. 5. Potential fault pattern in the region where the magnitude of deviatoric stress is greater than 50 MPa, $\alpha = 3.5^0$, $\beta = 10^0$, $k_4 = -1.5\rho_e g$, $k_8 = -100$ MPa, and $x_0 = 100$ km. The dash-dot line is the contour line of $\tau_{max} = 50$ MPa: (*a*) $\lambda = 0.4$, $\lambda_b = 0.9$, (*b*) $\lambda = 0.4$, $\lambda_b = 0.4$,(*c*) $\lambda = 0.0$, $\lambda_b = 0.4$, (*d*) $\lambda = 0.8$, $\lambda_b = 0.4$.

those used in Figure 5*a*. The thrust wedge under this condition can be divided into two parts: toward the toe, thrust faults are dominant, whereas toward the rear, normal faults are dominant. If the value k_4 is further reduced, the upper part of the wedge is occupied by thrust faults, whereas the basal part of the wedge is occupied by normal faults. This fault pattern is similar to what was observed in the classic Lewis thrust system, western Montana [*Yin and Kelty*, 1991]. The magnitude of deviatoric stress in nearly the entire wedge is less than 50 MPa. Because of this, the fault pattern predicted in this case can occur only if the wedge has a low fracture strength.

Variation of k_8 can also affect the state of stress in thrust wedges. Figure 7*a* shows the potential fault pattern in the region where the magnitude of deviatoric stress is greater than 50 MPa. I chose $k_8 = 0$ with all other parameters the same as those used in Figure 5a. We can see that the fault patterns in Figures 5*a* and 7*a* are quite similar. However, if we let $k_8 = -1000$ MPa, and all other parameters are the same as those used in Figure 5*a*, the normal faults in the upper part of Figure 5*a* are completely removed (Figure 7*b*). Note that $k_8 = -1000$ MPa is equivalent to assuming a deviatoric stress of 500 MPa, which is unrealistically high for the maximum deviatoric stress in the crust. This implies that for a long thrust wedge (in this case, 100 km), with the boundary conditions the same as those used in Figure 5*a*, normal faults are expected. However, if we let all the conditions used in Figure 5*a* be the same except assigning the length of the wedge $x_0 = 10$ km, we find that the entire wedge is dominated by thrusts (Figure 8). In this case, the magnitude of deviatoric stress in the entire wedge except the toe is less than 50 MPa. Concentration of deformation in the thrust toe is expected.

It has been suggested by numerous investigators [e.g.,

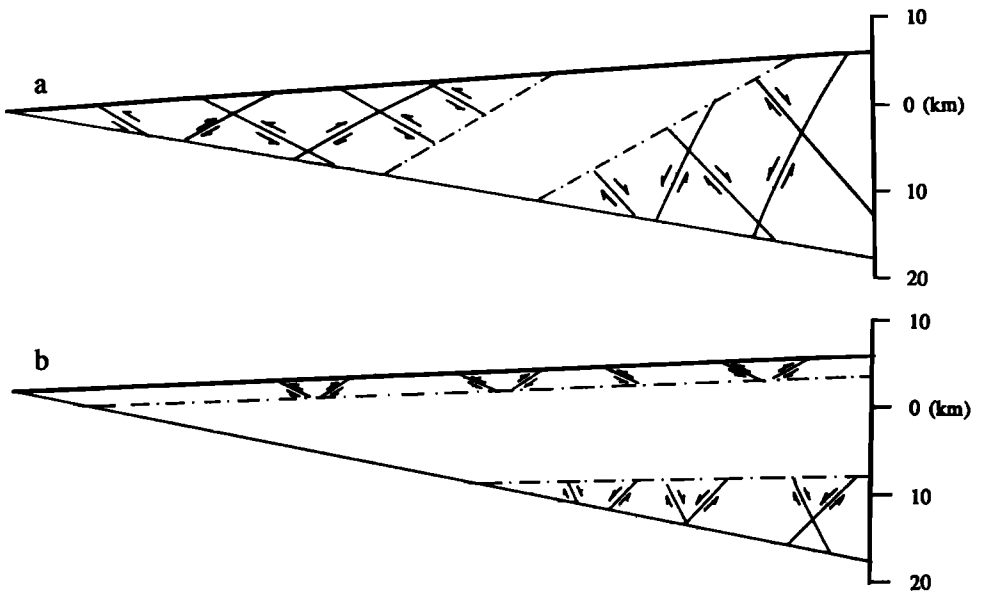

Fig. 6. Potential fault pattern where the magnitude of deviatoric stress is greater than 10 MPa, $\alpha = 3.5^0$, $\beta = 10^0$, $\lambda = 0.4$, $\lambda_b = 0.9$, $k_8 = -100$ MPa, and $x_0 = 100$ km. The dash-dotted line is the contour line of $\tau_{max} = 10$ MPa: (*a*) $k_4 = -0.5\rho_e g$, (*b*) $k_4 = 0.0$.

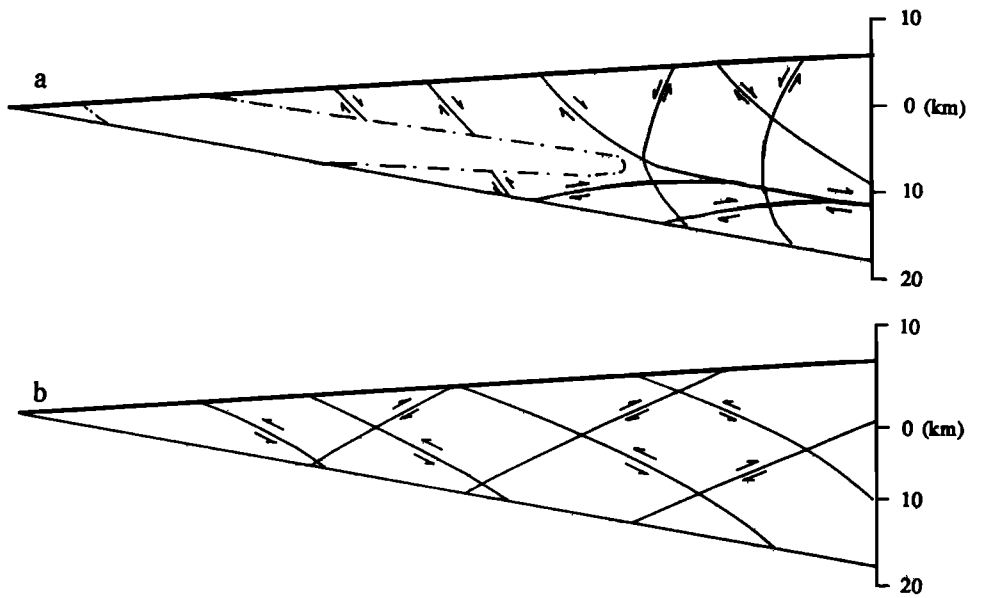

Fig. 7. Potential fault pattern in the region where the magnitude of deviatoric stress is greater than 50 MPa, $\alpha = 3.5^0$, $\beta = 10^0$, $\lambda = 0.4$, $\lambda_b = 0.9$, $k_4 = -1.5\rho_e g$, and $x_0 = 100$ km. The dash-dotted line is the contour line of $\tau_{max} = 50$ MPa: (*a*) $k_8 = 0$ MPa, (*b*) $k_8 = -1000$ MPa.

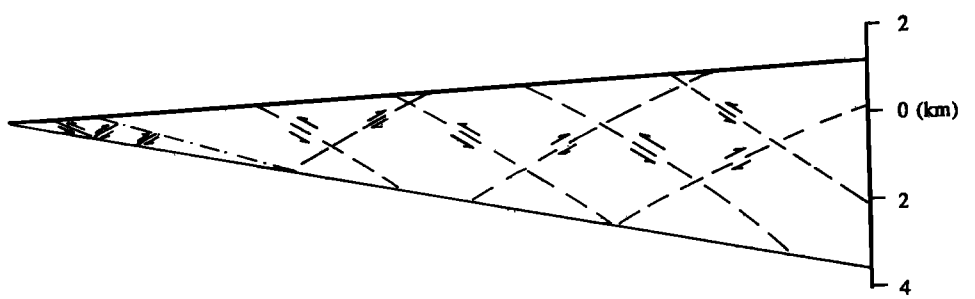

Fig. 8. Potential fault pattern for $\alpha = 3.5^0$, $\beta = 10^0$, $\lambda = 0.4$, $\lambda_b = 0.9$, $k_4 = -1.5\rho_e g$, $k_8 = -100$ MPa, and $x_0 = 10$ km. Solid lines represent potential faults in the area where the magnitude of deviatoric stress is greater than 50 MPa, whereas dashed lines represent faults in the area where the magnitude of deviatoric stress is less than 50 MPa. The dash-dotted line is the contour line of $\tau_{max} = 50$ MPa.

Platt, 1986] that the topographic slope is an important factor in determining whether the state of stress in a wedge is extensional or compressional. In particular, steeper slope should favor extension. Figure 9*a* shows that with all parameters the same as those in Figure 5*a*, except that the surface slope α is now 0^o, normal faults can still exist in the top part of the wedge. Faults are shown only in the region where the magnitude of deviatoric stress is greater than 50 MPa. This result indicates that the surface slope itself is not the only cause of horizontal extension. On the other hand, if the surface slope increases to $\alpha = 15^0$, which is unrealistic, normal faults prevail in the wedge above the horizonal (Figure 9*b*). If we keep all the parameters the same as those used in Figure 9*a* but increase the dip angle from $\beta = 10^0$ to $\beta = 50^0$, we find that the wedge is occupied by normal faults and subvertical faults (Figure 9*c*). The fault pattern in Figure 9*c* changes little, regardless of how pore fluid pressure ratios are assumed. This indicates that the geometry of the wedge, particularly the thrust dip, is an important factor in controlling the stress distribution in a thrust wedge.

In Figures 5 to 9, different curved fault shapes and senses of slip are implied. They include planar and listric, high-angle and low-angle, and normal and thrust faults. Such a variation in fault geometry has been observed in nature and may reflect the complex relationship between the mechanics of thrust wedges and boundary conditions.

Hubbert-Rubey Toes

The length of the Hubbert-Rubey toe is plotted against the dip angle of the basal thrust in Figure 10, in which $\lambda = 0.4$, $\lambda_b = 0.9$, $\alpha = 3.5^0$, and $k_4 = -1.5\rho_e g$ are assumed. A maximum length occurs at about $\beta = 10^0$. In general, the thicker the wedge is, the shorter its Hubbert-Rubey toe is for $\beta > 10^0$. Figure 10 also shows the importance of cohesive strength in controlling the length of the Hubbert-Rubey toe.

APPLICATIONS

The elastic wedge model described above may be applied to explain the formation of normal faults during the El Asnam thrust-type earthquake and the development of a Miocene north dipping normal fault system in the Higher Himalaya.

Structural Development During the El Asnam Earthquake

The El Asnam earthquake of October 10, 1980 (M_s 7.3), provided a wealth of geological and seismological data which have been used to aid our understanding of structural development of thrust-and-fold systems. Although the main event is clearly a thrust, widespread normal faults have been observed on the surface [*Yielding et al.*, 1981; *Philip and Meghraoui*, 1983]. In addition to the normal faults, fault plane solutions of the aftershocks both above and below the inferred thrust surface show thrusting [*Ouyed et al.*, 1983]. These observations suggest that normal faulting and thrusting are coeval in the same thrust wedge during the earthquake sequence.

Development of the normal faults has been explained either as a consequence of flexural slip folding [*Philip and Meghraoui*, 1983] or anticlinal uplifts during motion along the underlying thrust [*King and Vita-Finzi*, 1981; *Yielding et al.*, 1981] or as a complex deformational response of motion along flat ramp thrust [*Avouac et al.*, 1992]. *Avouac et al.* [1992] believe that folding itself cannot be the cause for the formation of all the observed normal faults, because the faults are found in places where no folds are developed. Considering that regional low-amplitude folds may not be observable, folding as a cause of normal faulting cannot be completely ruled out. The proposed flat ramp geometry for the thrust along which the main event occurred is an interesting alternative [*Avouac et al.*, 1992]. However, the aftershock pattern in the area strongly indicates that the fault is a relatively planar feature with its average dip angle between 40^o and 50^o (Figure 2) [*Ouyed et al.*, 1983; *Nabelek*, 1985]. The fault pattern predicted by the elastic wedge model is plotted in Figure 11 by using the dip angle $\beta = 45^0$ and the wedge length $x_0 = 12$ km. In this plot, pore fluid pressure ratios along the base and within the wedge are assumed to be $\lambda = \lambda_b = 0.4$, a uniform compressive stress of 100 MPa is applied (i.e., $k_8 = -100$ MPa), and $k_4 = -1.5\rho_e g$ is assigned. We find that the entire thrust wedge except the wedge tip favors the formation of normal faults. The tip of the wedge is under compression because at the point (0, 0), $\overline{\sigma}_{xx} = k_8 = -100MPa$. The prediction of thrusting near the tip of the thrust wedge and of extensive normal faulting away from the tip fits the observations well.

North Dipping Normal Faults in the Higher Himalaya

A north dipping normal fault system in the Higher (Greater) Himalaya was first reported in western literature by *Burg et al.* [1983] and *Burg and Chen* [1984]. *Burchfiel et al.* [1992] mapped extensively to further establish the position of the fault system and its relationship to regional structures. The results of their mapping suggest that the fault system can be traced along strike for at least 700 km and possibly traverses the entire 2000-km length of the Himalaya. The low-angle normal faulting probably initiated at 21 $\pm$1 Ma and may have lasted locally until as recently as about 11 Ma [*Copeland et al.*, 1988; *Maluski et al.*, 1988; *Hodges et al.*, 1991; *Burchfiel et al.*, 1992]. Coeval with the normal faulting in the Higher Himalaya was the development of the Main Central Thrust (MCT), the inverted metamorphic gradient in the footwall, and two-mica leucogranites in the hanging wall [*Hubbard and Harrison*, 1989; *Le Fort*, 1981; *Le Fort et al.*, 1987; *Copeland et al.*, 1990]. Initiation and development of the north dipping normal fault system previously was attributed to gravity sliding [*Berg and Chen*, 1984], gravitational collapse [*Burchfiel and Royden*, 1985], and southward directed ductile flow in the lower crust [*Yin, 1989*]. Although any one of these proposed causes may have been partially or completely responsible for the formation of the normal faults, the temporal and spatial association of (1) thrusting along the MCT, (2) intrusion of leucogranites, and (3) low-angle normal faulting in the hanging wall of the MCT hints at a causal relationship among them. As shown in Figure 5, high pore fluid pressure along the basal thrust favors compression in a thrust wedge, whereas low pore fluid pressure favors extension. This result may explain the relatively short life of the normal faulting. As proposed by *Le Fort* [1981], thrusting along the MCT led to juxtaposition of the hot hanging wall rocks (the Tibetan

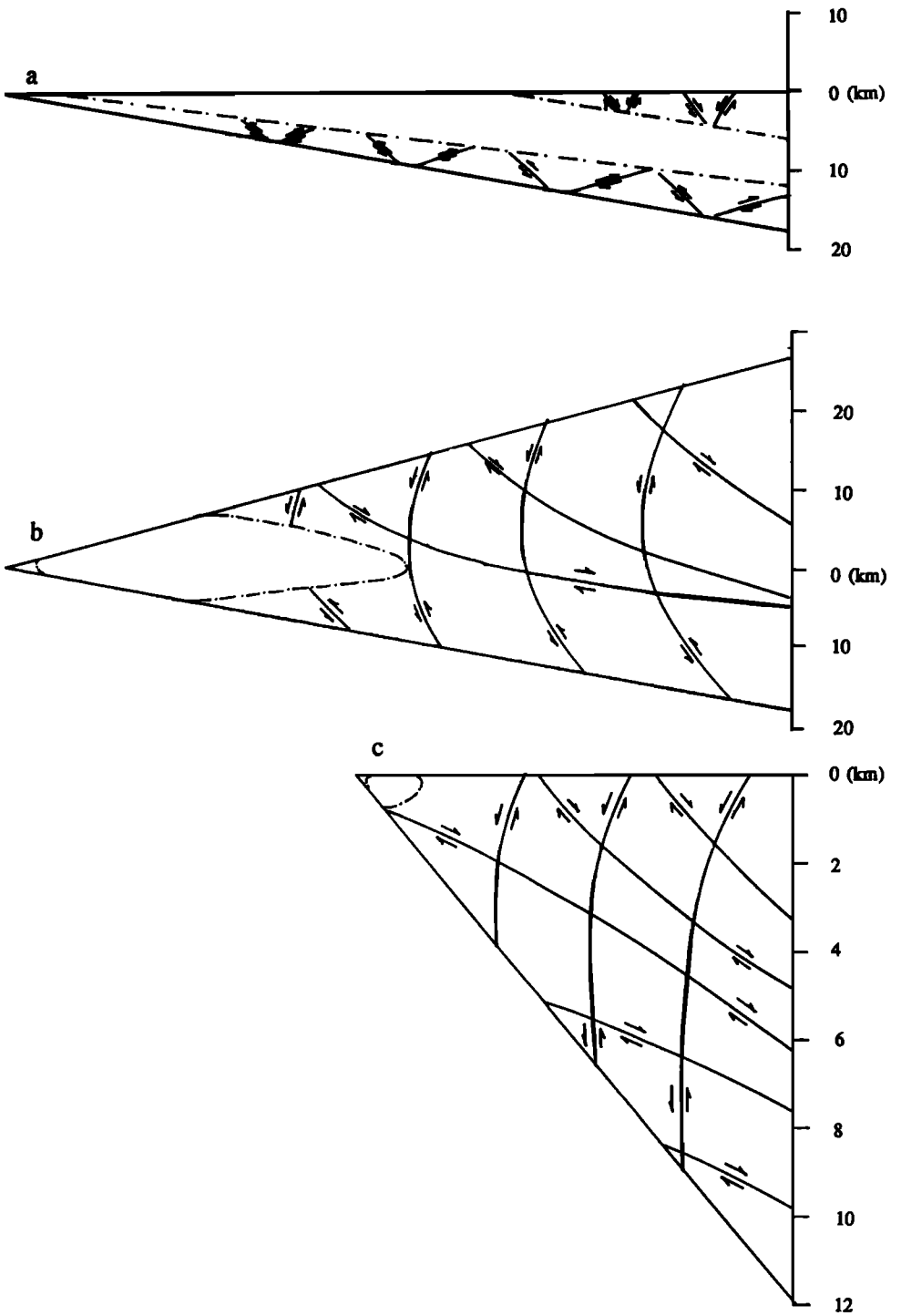

Fig. 9. Potential fault pattern in the region where the magnitude of deviatoric stress is greater than 50 MPa, $\lambda = 0.4$, $\lambda_b = 0.9$, $k_4 = -1.5\rho_e g$, $k_8 = -100$ MPa, and $x_0 = 100$ km. The dash-dotted line is the contour line of $\tau_{max} = 50$ MPa: (*a*) $\alpha = 0.0^0$, $\beta = 10^0$, (*b*) $\alpha = 15.0^0$, $\beta = 10^0$, (*c*) $\alpha = 0.0^0$, $\beta = 50^0$.

slab) over the cold footwall rocks (Midland Formations). This process may have induced dehydration reactions, defluidization, and devolatilization near the fault zone. As most of the fluids contributed to melting that formed the Himalayan leucogranites [*Le Fort et al.*, 1987], the pore fluid pressure along the MCT was reduced rapidly owing to the fast release of fluid. This in turn could have led to the reduction of basal friction and the initiation of the Higher Himalayan normal faults. The termination of normal faulting may have been related to the establishment of high pore fluid pressure along the Main Boundary Thrust (MBT) due to subduction of the Siwalik sediments. High fluid activity along the MBT during the early Pliocene has been inferred by *Copeland et al.* [1991]. The MBT lies structurally below the MCT between the Lesser Himalaya and Sub-Himalaya and is younger (post-middle Miocene [*Gansser*, 1981]). Because of smaller displacement along the MBT compared to the MCT on the basis of metamorphic grades juxtaposed by

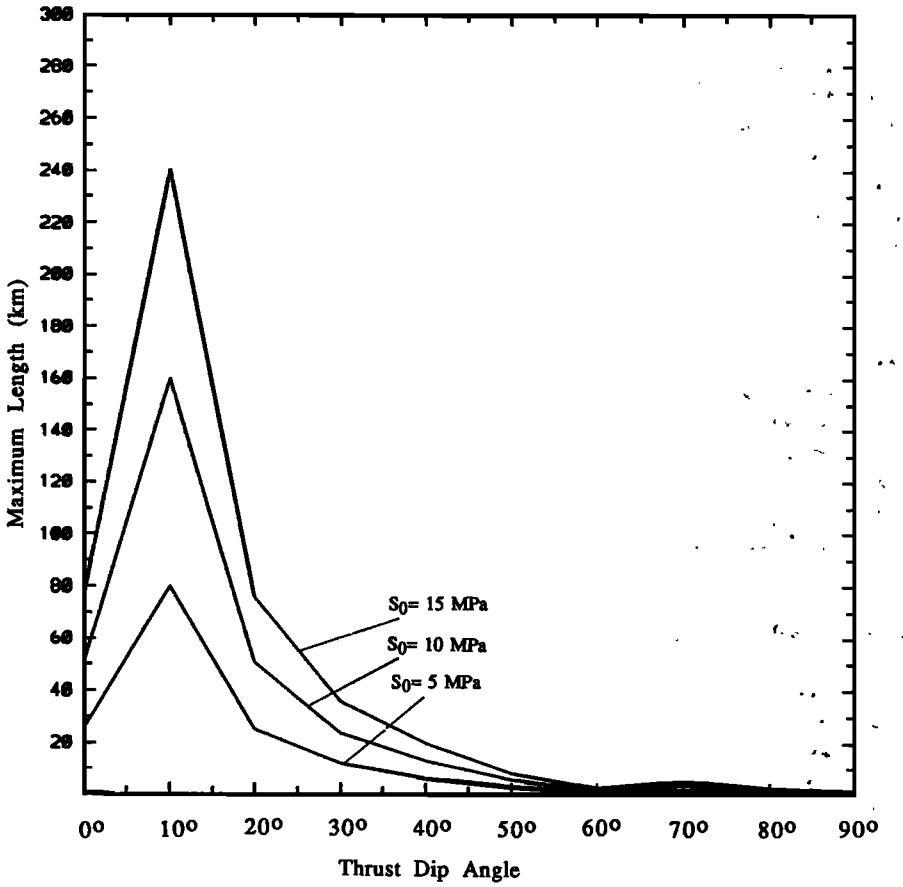

Fig. 10. Relation between the length of the Hubbert-Rubey toe, L, and the dip angle of the basal thrust β. Parameters used for this plot are $\alpha = 3.5^0$, $\lambda = 0.4$, $\lambda_b = 0.9$, $k_4 = -1.5\rho_e g$, and $k_8 = 0$. S_0 is the cohesive strength of the thrust wedge.

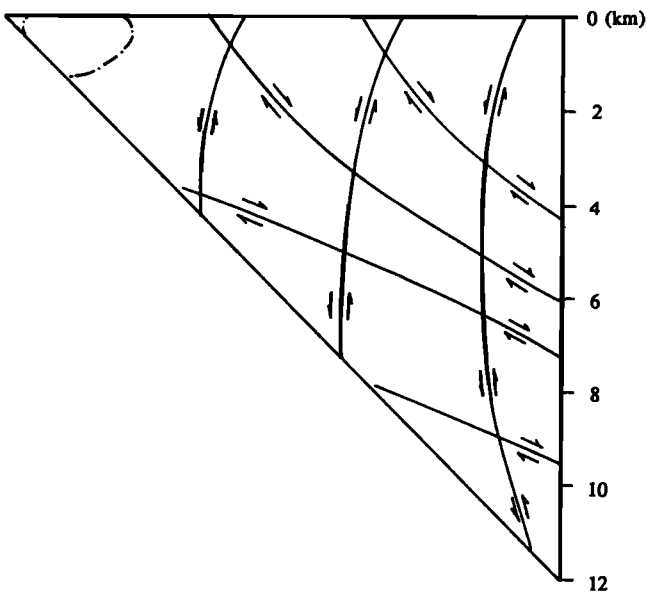

Fig. 11. Simulated fault pattern in the hanging wall of the El Asnam thrust. Thrust dip $\beta = 45^0$, $\lambda = \lambda_b = 0.4$, $k_8 = -100$ MPa, $k_4 = -1.5\rho_e g$, and $\alpha = 0^0$. The dash-dotted line is the contour line of $\tau_{max} = 50$ MPa.

the two faults, perhaps heat from the hanging wall of the MBT was not sufficient to cause extensive dehydration and defluidization along and adjacent to the MBT. This may explain why no post-MBT leucogranites and north dipping normal faulting developed in the Higher Himalaya.

DISCUSSION AND CONCLUSIONS

The boundary conditions in this study are similar to those used in the Coulomb wedge model [*Dahlen*, 1984]. However, the calculated stress distribution in elastic wedges is quite different from the Coulomb wedge model in that it implies simultaneous normal and thrust faults in the same thrust wedge and a listric geometry for both thrust and normal faults. The feature common to the two models is that they both suggest basal friction as the first-order control on the state of stress in thrust wedges. This is in strong contrast to the inference of *Platt* [1986] that the topographic slope decides whether the wedge is under extension or compression. Given that temperature, pressure, strain rate, and magnitude of stress vary by several orders of magnitude in the lithosphere; that the sizes of structures in consideration commonly differ drastically; and that the abundance of fractures/joints in the crust changes from place to place, it is impossible to use a single constitutive model to describe the mechanical behavior of all thrust wedges.

The model presented in this paper is applicable to both thick- and thin-skinned thrust wedges. It predicts that (1) lower friction along the base of thrust wedges can lead to dominantly horizontal compression in the wedge, whereas higher friction can lead to dominantly horizontal extension; (2) a long thrust wedge (>100 km) may have thrusts in

its lower portion and normal faults in its upper portion, even though a moderate to high compressive horizontal normal stress (100 MPa) is applied, whereas a short thrust wedge (< 10 km) can be entirely compressional under the same boundary conditions; (3) although an increase in topographic slope promotes horizontal extension, the limited range of its variation on a regional scale determines that it is less important than basal friction in producing extension; and (4) an increase in the vertical gradient of horizontal normal stress favors the development of normal faults in thrust wedges. The model is also used to calculate the length of the Hubbert-Rubey thrust toe, the unfractured, frontal portion of a thrust wedge. It shows that with the same boundary conditions, a narrower wedge in general has a longer Hubbert-Rubey thrust toe. The model is applied to explain the initiation of the Miocene normal fault system in the High Himalaya as a consequence of a rapid release of pore fluid pressure along the MCT during dewatering of sediments in the footwall and development of two-mica granites in the hanging wall. Termination of the north dipping normal faulting may have been related to initiation of the MBT along which high pore fluid pressure existed, favoring thrust wedge compression. The model also predicts the occurrence of normal faults associated with the El Asnam thrust-type earthquake.

Acknowledgments. The work presented here was part of my Ph.D. thesis under the supervision of Gregory A. Davis at the University of Southern California, whose geologic insight and encouragement during the course of this work are greatly appreciated. G. Davis, K. Aki, T. Henyey, C. Sammis, R. Walcott, and R. Burke offered valuable suggestions and discussion during the initial stage of this study. Dick Walcott's lectures on deformation of the continental lithosphere at USC during 1985 and 1986 inspired me to approach tectonic problems more quantitatively. Jack Dunn, Jay Jackson, and Tom Kelty are to be thanked for keeping my life in perspective while I was a graduate student. I thank T. M. Harrison, B. Hacker, D. Kemp, D. Young, and J. Fillipone for their valuable comments. I am grateful to P. Law for writing part of the plotting programs used in this research. Finally, penetrating reviews by the associate editor M. H. P. Bott and JGR reviewers R. Fletcher and R. Price are appreciated. The studies of Himalayan tectonics are supported by NSF grant EAR-9118125.

REFERENCES

Aki, K., and P.G. Richards, *Quantitative Seismology: Theory and Methods*, 932 pp., W.H. Freeman, New York, 1980.

Anderson, E.M., *The Dynamics of Faulting and Dyke Formation With Application to Britain*, 191 pp., Oliver and Boyd, Edinburgh, Scotland, 1942.

Avouac, J.P., B. Meyer, and P. Tapponnier, On the growth of normal faults and the existence of flats and ramps along the El Asnam active fold and thrust system, *Tectonics, 11*, 1-11, 1992.

Bally, A.W., P.L. Gordy, and G.A. Stewart, Structure, seismic data, and orogenic evolution of southern Canadian Rockies, *Bull. Can. Pet. Geol., 14*, 337-381, 1966.

Burg, J.P., F. Proust, P. Tapponnier, and G.M. Chen, Deformation phases and tectonic evolution of the Lhasa block (southern Tibet, China), *Eclogae Geol. Helv., 76*, 643-665, 1983.

Burg, J.P., and G.M. Chen, Tectonics and structural zonation of southern Tibet, China, *Nature, 311*, 219-223, 1984

Burchfiel, B.C., and L.H. Royden, North-south extension within the convergent Himalayan region, *Geology, 13*, 679-682, 1985

Burchfiel, B.C., et al., The south Tibetan detachment system, Himalayan orogen: Extension contemporaneous with and parallel to shortening in a collisional mountain belt, *Spec. Pap Geol. Soc. Am., 269*, 1-41, 1992.

Chapple, W.M., Mechanics of thin-skinned fold-and-thrust belts, *Geol. Soc. Am. Bull., 89*, 1189-1198, 1978.

Copeland, P., T.M. Harrison, K.V. Hodges, P. Maruejol, P. Le Fort, and A. Pecher, An early Pliocene thermal disturbance of the Main central thrust, central Nepal: Implications for Himalayan tectonics, *J. Geophys. Res., 96*, 8475-8500, 1991.

Copeland, P., T.M. Harrison, and P. Le Fort, Cooling history of the Manaslu granite, north-central Nepal, *Geol. Soc. Am. Abstr. Programs, 20*, 321, 1988.

Copeland, P., T.M. Harrison, and P. Le Fort, Age and cooling history of the Manaslu granite: Implications for Himalayan tectonics, *J. Volcanol. Geotherm. Res., 44*, 33-50, 1990.

Dahlen, F.A., Noncohesive critical Coulomb wedges: An exact solution, *J. Geophys. Res., 89*, 10,087-10,101, 1984.

Davis, D., J. Suppe, and F.A. Dahlen, Mechanics of fold-and-thrust belts and accretionary wedges, *J. Geophys. Res., 88*, 1153-1172, 1983.

De Bremaecker, J.C., Thrust sheet motion and earthquake mechanisms, *Earth Planet. Sci. Lett., 83*, 159-166, 1987.

Dewey, J.F., Extensional collapse of orogens, *Tectonics, 7*, 1,123-1,139, 1988.

Elliott, D., The motion of thrust sheets, *J. Geophys. Res., 81*, 949-963, 1976.

Emerman, S.H., and D.L. Turcott, A fluid model for the shape of accretionary wedges, *Earth Planet. Sci. Lett., 63*, 379-384, 1983.

Fletcher, R.C., Approximate analytical solutions for a cohesive fold-and-thrust wedge: Some results for lateral variation in wedge properties and for finite wedge angle, *J. Geophys. Res., 94*, 10,347-10,354, 1989.

Fung, Y.C., *Foundations of Solid Mechanics*, 593 pp., Chapman and Hall, London, 1965.

Gansser, A., *Geology of the Himalaya*, 289 pp., Wiley-Interscience, New York, 1964.

Gansser, A., The geodynamic history of the Himalaya, in *Zagros, Hindu Kush, Himalaya–Geodynamic Evolution, Geodyn. Ser.*, vol. 3, edited by H.K. Gupta and F.M. Delany, pp. 111-121, AGU, Washington, D.C., 1981.

Hafner, W., Stress distribution and faulting, *Geol. Soc. Am. Bull., 62*, 373-398, 1951.

Harrison, T.M., P. Copeland, W.S.F. Kidd, and A. Yin, Raising Tibet, *Science, 255*, 1663-1670, 1992.

Hodges, K., B.C. Burchfiel, Z. Chen, T. Housh, D. Lux, R. Parrish, and L.H. Royden, Rapid early Miocene tectonic unroofing of the metamorphic core of the Himalaya: Evidence from the Qomolangma (Everest) region, Tibet, *Geol. Soc. Am. Abstr. Programs, 23*, 372, 1991.

Hubbard, M. S., and T.M. Harrison, $^{40}Ar/^{39}$ Ar age constraints on deformation and metamorphism in the Main Central Thrust zone and Tibetan slab, eastern Nepal, Himalaya, *Tectonics, 8*, 865-880, 1989.

Hubbert, M.K., and W.W. Rubey, Role of fluid pressure in mechanics of overthrust faulting, I, Mechanics of fluid-filled porous solids and its application to overthrust faulting, *Geol. Soc. Am. Bull., 70*, 115-166, 1959.

Jaeger, J.C., and N.G.W. Cook, *Fundamentals of Rock Mechanics*, 593 pp., Chapman and Hall, London, 1979.

King, G.P.C., and C. Vita-Finzi, Active folding in the Algerian earthquake of 10 October 1980, *Nature, 292*, 22-26, 1981.

King, G., and G. Yielding, The evolution of a thrust fault system: Process of rupture initiation, propagation, and termination in the 1980 El Asnam (Algeria) earthquake, *Geophys. J. R. Astron. Soc., 77*, 915-933, 1984.

Le Fort, P., Manaslu leucogranite: A collision signature of the Himalaya-A model for its genesis and emplacement, *J. Geophys. Res., 86*, 10,545-10,568, 1981.

Le Fort, P., M. Cuney, C. Deniel, C. France-Lanord, S.M.F. Sheppard, B.N. Upreti, and P. Vidal, Crystal generation of the Himalayan leucogranites, *Tectonophysics, 134*, 39-57, 1987.

Liu, J.Y., and G. Ranalli, Stress in an overthrust sheet and propagation of thrusting: An Airy stress function solution, *Tectonics, 11*, 549-559, 1992.

Lyon-Caen, H., and P. Molnar, Constraints on the structure of the Himalaya from an analysis of gravity anomolies and a flexural model of the lithosphere, *J. Geophys. Res., 88*, 8171-8191, 1983.

Maluski, H., P. Matte, and M. Brunel, Argon 39 - Argon 40 dating of metamorphic and plutonic events in the North and High Himalayas belts (southern Tibet-China), *Tectonics, 7*, 299-326, 1988.

McGarr, A., and N.C. Gay, State of stress in the Earth's crust, *Annu. Rev. Earth Planet. Sci., 6*, 405-436, 1978.

Nabelek, J., Geometry and mechanism of faulting of the 1980 El Asnam, Algeria, earthquake from inversion of teleseismic body waves and comparison with field observations, *J. Geophys. Res., 90*, 12,713-12,728, 1985.

Ni, J., and M. Barazangi, Seismotectonics of the Himalayan collision zone: Geometry of the underthrusting Indian plate beneath the Himalaya, *J. Geophys. Res., 89*, 1147-1163, 1984.

Ouyed, M., G. Yielding, D. Hatzfeld, and G.C.P. King, An aftershock study of El Asnam (Algeria) earthquake of 1980, *Geophys. J. R. Astron. Soc., 73*, 605-639, 1983.

Philip, H., and M. Meghraoui, Structural analysis and interpretation of the surface deformation of the El Asnam earthquake of October 10, 1980, *Tectonics, 2*, 17-49, 1983.

Platt, J.P., Dynamics of orogenic wedges and the uplift of high-pressure metamorphic rocks, *Geol. Soc. Am. Bull., 97*, 1037-1053, 1986.

Price, R.A., Large scale gravitational flow of supra- crustal rocks, Southern Canadian Rockies, in *Gravity and Tectonics*, edited by K.A. de Jong and R. Scholten, pp. 491-502, John Wiley, New York, 1973*a*.

Price, R.A., The mechanical paradox of large overthrusts, *Geol. Soc. Am. Abstr. Program, 5*, 772, 1973*b*.

Price, R.A., The Cordilleran foreland thrust-and-fold belt in the Southern Canadian Rocky Mountains, in Thrust and Nappe Tectonics, edited by K.J. McClay and N.J. Price, *Geol. Soc. London Spec. Publ., 9*, 427-448, 1981.

Price, R.A., The mechanical paradox of large overthrusts, *Geol. Soc. Am. Bull., 100*, 1898-1908, 1988.

Reade, T.M., The mechanics of overthrusts, *Geol. Mag., 5*, 518, 1908.

Seeber, L., J.G. Armbruster, and R.C. Quittmeyer, Seismicity and continental subduction in the Himalayan arc, in *Zagros, Hindu Kush, Himalaya Geodynamic Evolution, Geodyn. Ser.*, vol. 3, edited by H.K. Gupta and F.M. Delany, pp. 215-242, AGU, Washington, D.C., 1981.

Smoluchowski, M.S., Some remarks on the mechanics of overthrusts, *Geol. Mag., 6*, 204-205, 1909.

Stockmal, G.S., Modeling of large-scale accretionary wedge deformation, *J. Geophys. Res., 88*, 8271-8287, 1983.

Suppe, J., *Principles of Structural Geology*, Prentice-Hall, Englewood Cliffs, N.J., 1985.

Xiao, H.B., F.A. Dahlen, and J. Suppe, Mechanics of extensional wedges, *J. Geophys. Res., 96*, 10,301-10,328, 1991.

Yielding, G., J.A. Jackson, G.C.P. King, H. Sinvhal, C. Vita-Finzi, and R.M. Wood, Relation between surface deformation, fault geometry, seismicity and rupture characteristics during the El Asnam (Algeria) earthquake of 10 October 1980, *Earth Planet. Sci. Lett., 56*, 287-304, 1981.

Yin, A., A mechanical model for a wedge-shaped thrust sheet, *Eos Trans. AGU, 67*, 1242, 1986.

Yin, A., Geometry, kinematics, and a mechanical analysis of a strip of the Lewis allochthon from Peril Peak to Bison Mountain, Glacier National Park, Montana, Ph.D dissertation, 290 pp., Univ. of South. Calif., Los Angeles, 1988.

Yin, A., Origin of regional, rooted low-angle normal faults: A mechanical model and its tectonic implications, *Tectonics, 8*, 469-482, 1989.

Yin, A., and T.K. Kelty, Development of normal faults during emplacement of a thrust sheet: An example from the Lewis allochthon, Glacier National Park, Montana, *J. Struct. Geol., 13*, 37-47, 1991.

A. Yin, Department of Earth and Space Sciences, University of California, Los Angeles, CA 90024.

(Received August 13, 1993;
revised March 5, 1993
accepted March 5, 1993.)